Cell Reports
Physical Science

CellPress
OPEN ACCESS

Article

Field-coupling topology design of general transformation multiphysics metamaterials with different functions and arbitrary shapes

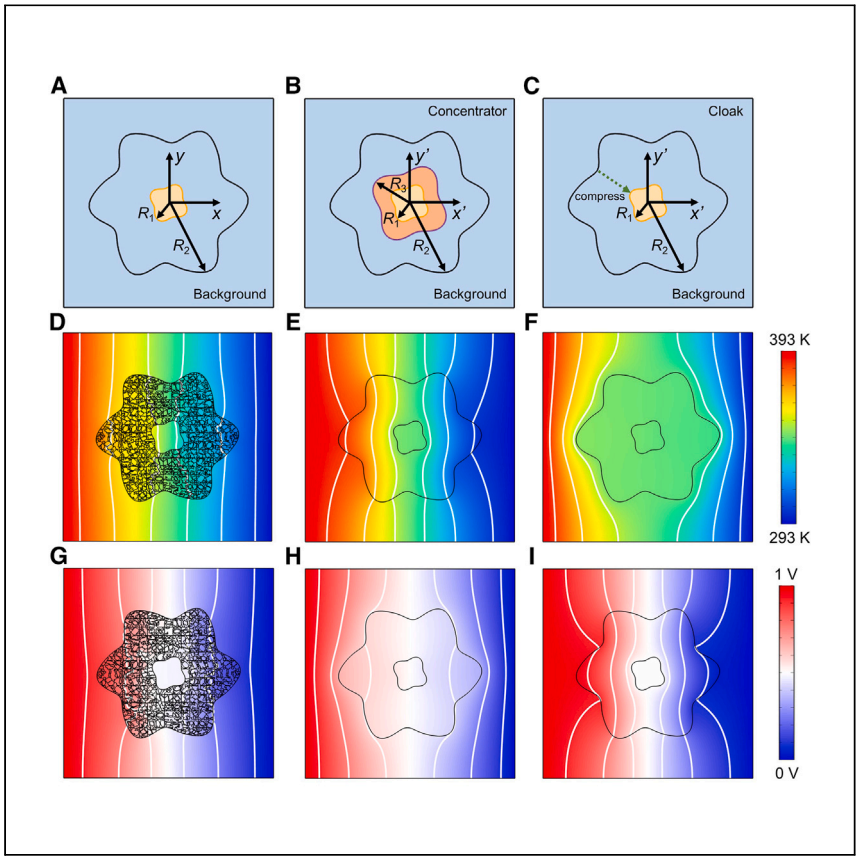

Metamaterials have been extensively studied due to their exciting properties, broad physics, and promising applications covering a vast range of science and engineering; however, most metamaterials only focus on a single physical field. Zhu et al. propose arbitrary-shape transformation multiphysics metamaterials capable of manipulation of heat and electric current for different combinations of cloaking/concentrating functions.

Zhan Zhu, Zhaochen Wang, Tianfeng Liu, Xiaobing Luo, Chengwei Qiu, Run Hu

hurun@hust.edu.cn

Highlights

General arbitrary-shape transformation multiphysics metamaterials are proposed

Multiphysics metamaterials to manipulate both heat and electric current are designed

A roadmap is presented to design multiphysics metamaterials with a range of functionality

Zhu et al., Cell Reports Physical Science 4, 101540
August 16, 2023
https://doi.org/10.1016/j.xcrp.2023.101540

Please cite this article in press as: Zhu et al., Field-coupling topology design of general transformation multiphysics metamaterials with different functions and arbitrary shapes, Cell Reports Physical Science (2023), https://doi.org/10.1016/j.xcrp.2023.101540

Cell Reports
Physical Science

Article

Field-coupling topology design of general transformation multiphysics metamaterials with different functions and arbitrary shapes

Zhan Zhu,[1] Zhaochen Wang,[1] Tianfeng Liu,[1] Xiaobing Luo,[1] Chengwei Qiu,[2] and Run Hu[1,3,*]

SUMMARY

Metamaterials have been extensively studied due to their exciting properties, broad physics, and promising applications covering a vast range of science and engineering. However, most metamaterials only focus on a single physical field rather than multiphysics fields, which limits their interdisciplinary applications, and existing multiphysics metamaterials usually have the same functions. Here, we propose general arbitrary-shape transformation multiphysics metamaterials (TMM) based on a discretion-and-assembly strategy. As proof-of-concept, we designed several arbitrary-shape TMMs to achieve the robust manipulation of heat and electric current for different combinations of cloaking/concentrating functions. The recipe of the general TMM includes coupling the multiphysics anisotropic parameters, offering a general strategy to fabricate metamaterials, endowing the shape flexibility, and enabling the functionality robustness. Our study offers a general way to design TMMs with anisotropic material properties and paves a new way to design multiphysics metamaterials across multiple disciplines.

INTRODUCTION

Metamaterials are artificially structured materials with extraordinary properties, which have been extended from electromagnetics and optics[1,2] to acoustics,[3,4] thermotics,[5–12] and mechanics,[13–15] and exhibited great potential on manipulating wave or flux in multiphysics fields. Tremendous advances in metamaterials have been witnessed during the past decade, triggering the booming manners of functions like cloaking,[16–22] concentrating,[23–27] rotating,[28] reflecting,[29] illusion,[30–32] camouflage,[33,34] printing,[35] encoding,[36] and so on. However, most of these metamaterials only work in a particular physical field rather than multiphysics fields. For example, the designed thermal metadevice can only manipulate heat flux, and the designed electric metadevice can only control the electric current. The key challenge is that different physical fields are usually described by different governing equations and material parameters, like the thermal conductivity (κ) in thermotics and the electric conductivity (σ) in electrics. Thanks to the same-form Laplace governing equations in thermotics and electrics, i.e., $\nabla\cdot(\kappa\nabla T) = 0$ and $\nabla\cdot(\sigma\nabla V) = 0$, where T and V are the temperature and electric potential, respectively, it is relatively easy to design multiphysics metamaterials with the same function in thermal and electrical fields, such as thermal/electric cloaking and thermal/electric concentrating.[37] The same-form governing equation and the transformation theory for same function only require a constant ratio between κ and σ in the design domain of metamaterials, which significantly simplifies the process of material selecting and structure designing to some extent. Due to quasi-linear correlation between κ and σ,

[1]School of Energy and Power Engineering, Huazhong University of Science and Technology, Wuhan 430074, China

[2]Department of Electrical and Computer Engineering, National University of Singapore, Kent Ridge 117583, Republic of Singapore

[3]Lead contact

*Correspondence: hurun@hust.edu.cn

https://doi.org/10.1016/j.xcrp.2023.101540

Please cite this article in press as: Zhu et al., Field-coupling topology design of general transformation multiphysics metamaterials with different functions and arbitrary shapes, Cell Reports Physical Science (2023), https://doi.org/10.1016/j.xcrp.2023.101540

achieving the same functions for both thermal and electric fields is relatively easy.[38,39] However, to achieve multiphysics metamaterials with different functions is rather challenging, as the required local parameters are distinct spatially, even contradictory and rival. For instance, the thermal cloaking requires that tangential κ is approaching infinite and radial κ is approaching zero, while the electric concentrating requires that tangential σ is approaching zero and radial σ is approaching infinite. Such contradictory requirement is rather scarcely possible to find the same constitutive materials due to the quasi-linear correlation between κ and σ. In this paper, we present a general roadmap to design arbitrary-shape transformation multiphysics metamaterials (TMM), and as proof-of-concept design several TMMs to demonstrate the combinations of different functions in thermal and electric fields simultaneously.

To start, we would like to clarify the difference of designing multiphysics metamaterials between the same function and different functions. For the same function, say annular thermal cloaking and electric cloaking, we transform the circular space $r \leq R_2(\theta)$ into the annular one $R_1(\theta') \leq r' \leq R_2(\theta')$, and thus the Jacobian matrix $\boldsymbol{J}$ during the coordinate transformation stays the same for different fields, yielding the following transformed thermal and electric conductivities:

$$\begin{bmatrix} \tilde{\kappa} \\ \tilde{\sigma} \end{bmatrix} = \frac{\boldsymbol{J}\boldsymbol{J}^{\dagger}}{det(\boldsymbol{J})} \begin{bmatrix} \kappa_b \\ \sigma_b \end{bmatrix} = \boldsymbol{F}(r', \theta') \begin{bmatrix} \kappa_b \\ \sigma_b \end{bmatrix} \quad \text{(Equation 1)}$$

where the coefficient matrix $\boldsymbol{F}(r', \theta')$ is quantified by the coordinate transformation between the virtual and real space according to the desired functions. Therefore, for same functions, we have $\tilde{\kappa}/\tilde{\sigma} = \kappa_b/\sigma_b$ throughout the design domain, which actually offers convenience in fabricating multiphysics metamaterials. Such annular multiphysics cloak designed by transformation theory is inhomogeneous and anisotropic, which are difficult for fabrication. Alternatively, annular multiphysics cloak designed by the scattering cancellation technique, as shown in Figure 1E, the conductivity ratio is $\frac{\kappa_s}{\kappa_b} = \frac{\sigma_s}{\sigma_b} = \frac{R_2^2+R_1^2}{R_2^2-R_1^2}$ where R_1 and R_2 are the inner and external radii of the annular shell. This implies that $\kappa_s/\sigma_s = \kappa_b/\sigma_b$ as well throughout the design domain. Such material requirement of equal $\tilde{\kappa}/\tilde{\sigma}$ throughout the cloak and the background is rather stringent, which severely limits the flexibility of materials selection and the practicality of experimental application. Moreover, the scattering cancellation technique, originated from the source-free plane wave solution to the Laplace equations, only offers the design of global effective properties in the shell region rather than designing local properties, and thus offers fewer functions and shape flexibility than the transformation theory, let alone metamaterials with different functions. Another problem with the annular structure is the thermal resistance between different layers, since the material of different layers is usually different.

To design multiphysics metamaterials with different functions, say thermal concentrating and electric cloaking, the coordinate transformations and the corresponding Jacobian matrixes are different. For thermal concentrating we compress the region $r \leq R_3(\theta)$ into $r' \leq R_1(\theta')$ and extend the region $R_3(\theta) \leq r \leq R_2(\theta)$ to $R_1(\theta') \leq r' \leq R_2(\theta')$, while for electric cloaking we transform the space $r \leq R_2(\theta)$ in the virtual space into the annular one $R_1(\theta') \leq r' \leq R_2(\theta')$ in the real space. Therefore, different coordinate transformations lead to different Jacobian matrix $\boldsymbol{J}$ and $\boldsymbol{J}'$. The transformed thermal and electric conductivities are:

$$\begin{bmatrix} \tilde{\kappa} \\ \tilde{\sigma} \end{bmatrix} = diag\left[\frac{\boldsymbol{J}'\boldsymbol{J}'^{\dagger}}{det(\boldsymbol{J}')}, \frac{\boldsymbol{J}\boldsymbol{J}^{\dagger}}{det(\boldsymbol{J})}\right] \begin{bmatrix} \kappa_b \\ \sigma_b \end{bmatrix} = diag[\boldsymbol{G}(r', \theta'), \boldsymbol{F}(r', \theta')] \begin{bmatrix} \kappa_b \\ \sigma_b \end{bmatrix} \quad \text{(Equation 2)}$$

Please cite this article in press as: Zhu et al., Field-coupling topology design of general transformation multiphysics metamaterials with different functions and arbitrary shapes, Cell Reports Physical Science (2023), https://doi.org/10.1016/j.xcrp.2023.101540

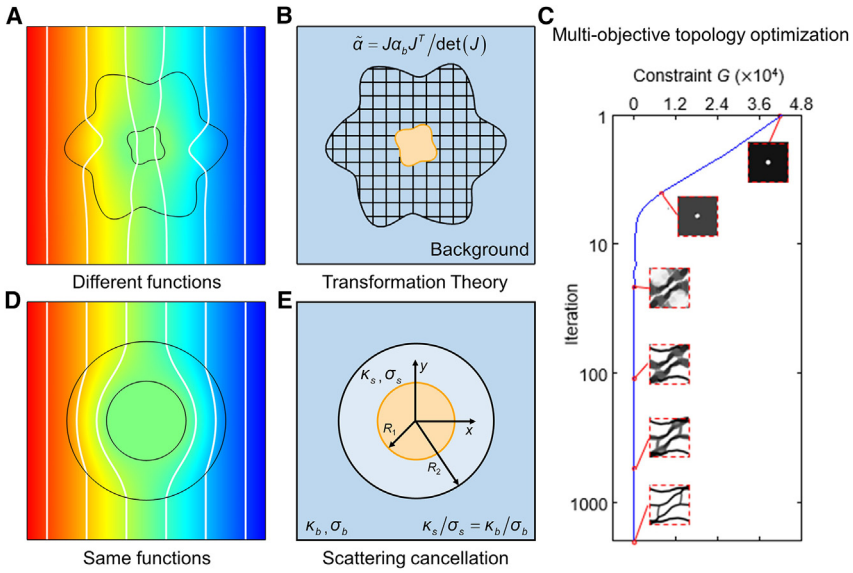

Figure 1. Design of arbitrary-shape TMM with different functions

(A) Thermal-electric field of TMM with thermal cloaking (color gradient) and electric concentrating (equipotential lines).

(B) Schematic of the discretion-and-assembly strategy of arbitrary-shape TMM.

(C) FCTO routine of one TFC.

(D) Thermal-electric field of conventional multiphysics metamaterials with thermal cloaking (color gradient) and electric cloaking (equipotential lines).

(E) Schematic of the annular cloak designed by scattering cancellation technique.

where the coefficient matrixes $\boldsymbol{G}(r',\theta')$ and $\boldsymbol{F}(r',\theta')$ are different according to the concentrating and cloaking functions. Therefore, the ratio $\tilde{\kappa}/\tilde{\sigma}$ differs spatially from coordinate to coordinate, i.e., $\tilde{\kappa}/\tilde{\sigma} = \kappa_b/\sigma_b \cdot \frac{\boldsymbol{G}(r',\theta')}{\boldsymbol{F}(r',\theta')}$. Moreover, the conductivity $\tilde{\kappa}$ and $\tilde{\sigma}$ are tensor actually, and then their components are also different spatially. More discussions on $\tilde{\kappa}/\tilde{\sigma}$ with different functions are presented in Note S1 and Figure S1. Such spatially varying $\tilde{\kappa}/\tilde{\sigma}$ and their components make it nearly infeasible to precisely design multiphysics metamaterials with different functions by bulk materials.

RESULTS

Methodology

To solve this problem, we propose a discretion-and-assembly strategy, namely dividing the design domain into many topological functional cells (TFCs), calculating the desired $\tilde{\kappa}$ and $\tilde{\sigma}$ by the general transformation theory with different functions, optimizing the local structures of each TFC by a multi-objective topology optimization, and assembling TFCs into arbitrary-shape metamaterials for different function demonstration. As we employ the general transformation theory rather than scattering cancellation method, the designed multiphysics materials are specifically addressed as TMM hereinafter. As shown in Figure 1B, we divide the TMM into many square TFCs, each of which takes the transformed conductivity tensor of the central point calculated by the transformation theory as the target conductivity α (=κ or σ). The number of TFCs will influence the accuracy of the target functions and the difficulty of the design and fabrication. With the increase in the number of TFCs, the accuracy of the target functions will be enhanced, but the design and fabrication become more difficult. Therefore, a trade-off is suggested to choose a reasonable number of TFCs. The accuracy of achieving the local α depends on the size of square

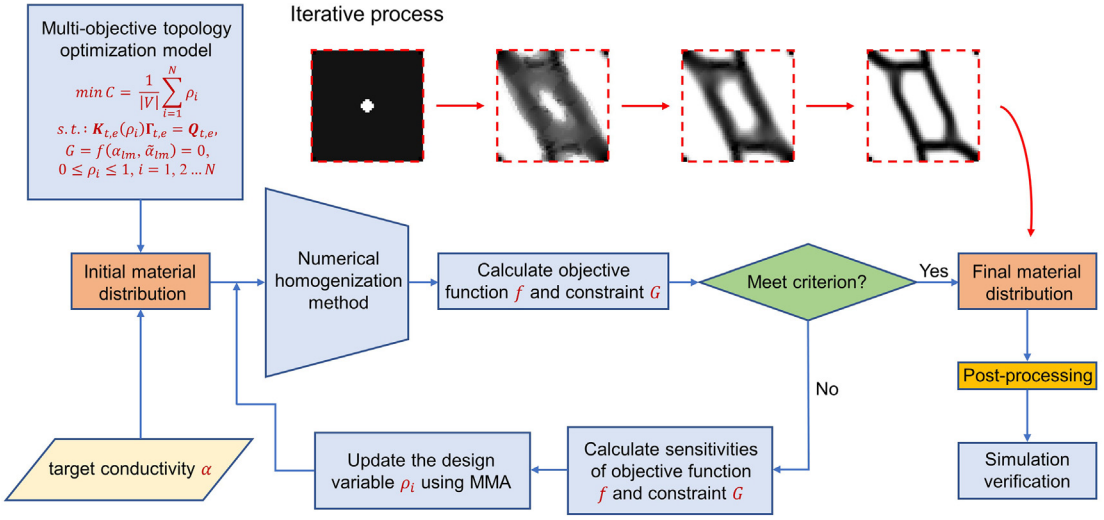

Figure 2. Flow chart of the field-coupling topology optimization roadmap

cells and the inverse optimization algorithm. Here, field-coupling topology optimization (FCTO) is employed specifically to design the $\tilde{\kappa}$ and $\tilde{\sigma}$ simultaneously by taking the transformed tensor α as the objective. The flow chart of FCTO roadmap is shown in Figure 2. To inversely design from specific properties to material distribution in these TFCs, we must figure out how material distribution determines material properties. Here, we mesh each TFC into *N* finite elements and calculate its effective conductivities by the numerical homogenization method.[40] In numerical homogenization, the periodic boundary condition is commonly used. The thermal/electric conductivity tensor α_{lm} (l, m = 1, 2) of each TFC can be calculated as

$$\alpha_{lm} = \begin{bmatrix} \alpha_{11} & \alpha_{12} \\ \alpha_{21} & \alpha_{22} \end{bmatrix} = \frac{1}{|V|}\sum_{i=1}^{N}\left(\Delta\Gamma_i^l\right)^{\dagger}\Lambda_i(\rho_i)\Delta\Gamma_i^m \qquad \text{(Equation 3)}$$

where $|V|$ is the total volume of each TFC. $\Delta\Gamma_i$ (= $\Gamma_i^0 - \Gamma_i$) is the temperature/potential vector difference where Γ_i^0 is the nodal temperature/potential vector under the uniform test heat/electric current $\mathbf{q}_i^0$, and Γ_i is the induced nodal temperature/potential field. $\Lambda_i(\rho_i) = \alpha(\rho_i)\Lambda_i^0$ is the conductivity matrix determined by the conductivity coefficient $\alpha(\rho_i)$ of each finite element and the unit conductivity matrix $\Lambda_i^0 = \int_{V_i}\left[\left(\frac{\partial \mathbf{N}}{\partial x}\right)^{\dagger}\left(\frac{\partial \mathbf{N}}{\partial x}\right) + \left(\frac{\partial \mathbf{N}}{\partial y}\right)^{\dagger}\left(\frac{\partial \mathbf{N}}{\partial y}\right)\right]dV_i$, where N is the shape function and V_i is the volume of a finite element. In topology optimization,[41,42] each finite element is assigned an artificial continuous density ranging from 0 to 1, which is taken as the design variable during the iterative process. Here, we employ a modified solid isotropic material with penalization scheme to interpolate the design variables to material properties of two materials, i.e., $\alpha(\rho_i) = \alpha_{\text{material 1}} + \rho_i^p(\alpha_{\text{material 2}} - \alpha_{\text{material 1}})$, where p is the penalty coefficient and ρ_i is the effective density of each finite element in a range of 0 and 1. To improve the accuracy, the effective density should be close to either 0 or 1, and the penalty coefficient p is set to 5 properly after initial tests. In our design, four corners in each topological functional cell are set as 1 to make sure each cell is connected to each other. This setup greatly improves the connectivity between cells. This is also another merit of our metamaterial over traditional multilayer structures. With reasonable selections of objective function and constraint, the design variable ρ_i can be updated iteratively until obtaining a satisfying topological structure to achieve the required properties. Here, the multi-objective topology optimization model for obtaining the desired tensor α is formulated as

$$\begin{cases} \min C = \dfrac{1}{|V|}\sum_{i=1}^{N}\rho_i \\ s.t.: K_{t,e}(\rho_i)\Gamma_{t,e} = Q_{t,e}, \\ G = f(\alpha_{lm}, \tilde{\alpha}_{lm}) = 0, (l, m = 1, 2) \\ 0 \le \rho_i \le 1, i = 1, 2 \ldots N \end{cases} \quad \text{(Equation 4)}$$

where $f(\ldots)$ is a custom function to evaluate the difference between the effective properties of the optimized configuration α_{lm} and the input properties $\tilde{\alpha}_{lm}$ of each TFC. $K_{t,e}(\rho_i)$, $\Gamma_{t,e}$, and $Q_{t,e}$ are the global heat/electric conduction matrix, global temperature/potential matrix, and global thermal/electric load matrix, respectively. $K_{t,e}(\rho_i)$ and $Q_{t,e}$ can be quantified by $K_{t,e}(\rho_i) = \sum_{i=1}^{N}\Lambda_i$ and $Q_{t,e} = \sum_{i=1}^{N} N q_i^0$, respectively. It should be noted that we set minimizing the volume fraction of material 2 as the objective function, take the difference between α_{lm} and $\tilde{\alpha}_{lm}$ as the constraint, to make the optimization process more effective. The sensitivities of constraint G and objective function C, i.e., the derivative of constraint G and objective function C with respect to design variable, can be calculated by using the adjoint method. Then, the design variable ρ_i will be updated on the basis of the sensitivities with the method of moving asymptotes (MMA).[43] By introducing moving asymptotes, the MMA method transforms the implicit optimization problem into a series of explicitly simpler and strictly convex approximate suboptimization problems. In each iteration step, new design variables are obtained by solving an approximately convex subproblem. Inputting the required properties of each TFC calculated from the transformation theory, the topological configuration of each TFC can be obtained by optimizing the design variable ρ_i. The evolution of topology optimization process of one typical TFC is plotted in Figure 1C. The material distribution in the TFC is increasingly clearer after a certain number of iterations, since the design variable ρ_i is updated iteratively. The optimization stops when the constraint G is small enough, i.e., the effective properties of the TFC are close to target input properties. Through FCTO, the topological configuration of each discrete TFC in TMMs can be optimized to achieve the target conductivity calculated by the transformation theory. Through this method, the TFC with varying $\tilde{\kappa}/\tilde{\sigma}$ can be designed with acceptable error by either selecting proper materials or adjusting the distribution of materials. For more discussion on the varying $\tilde{\kappa}/\tilde{\sigma}$, refer to Note S2 and Figures S2 and S3. After obtaining the 0–1 material distribution of each TFC, we can assemble TFCs into the complete multiphysics metamaterials by integrating the TFCs into a larger 0–1 matrix, which can represent the whole metamaterials. Furthermore, the geometry of the multiphysics metamaterials can be imported by COMSOL Multiphysics 5.5 with MATLAB for subsequent simulations and optimizations. Since each TFC of TMMs locally achieve the target thermal/electric conductivity, the whole TMMs can realize the specific functions in different physical fields. To validate the effectiveness of the discretion-and-assembly strategy, we first evaluate whether the TFCs possess the desired anisotropic parameters. As shown in Figure 3, temperature and potential are almost identical for the target fields and TFC fields, which verify the TFCs with the target properties.

Design and verification

To verify our general roadmap, we first design a TMM with thermal concentrating and electric cloaking function in a single device. For general, the arbitrary shapes of the TMM are described by two parameterized curves with respect to azimuth coordinate θ, as shown in Figures 4A–4C, as $R_1 = 0.75[1.5\cos(4\theta + 2\pi/3) + 10]$, $R_2 = 2[0.3\sin(12\theta) + 2\cos(6\theta) + 15]$, and $R_3 = 2[1.5\cos(4\theta + 2\pi/3) + 10]$, where R_3 is used for thermal concentrating only. The whole region is discretized into 25 × 25 cells, and each cell is discretized into 100 × 100 square finite elements

Please cite this article in press as: Zhu et al., Field-coupling topology design of general transformation multiphysics metamaterials with different functions and arbitrary shapes, Cell Reports Physical Science (2023), https://doi.org/10.1016/j.xcrp.2023.101540

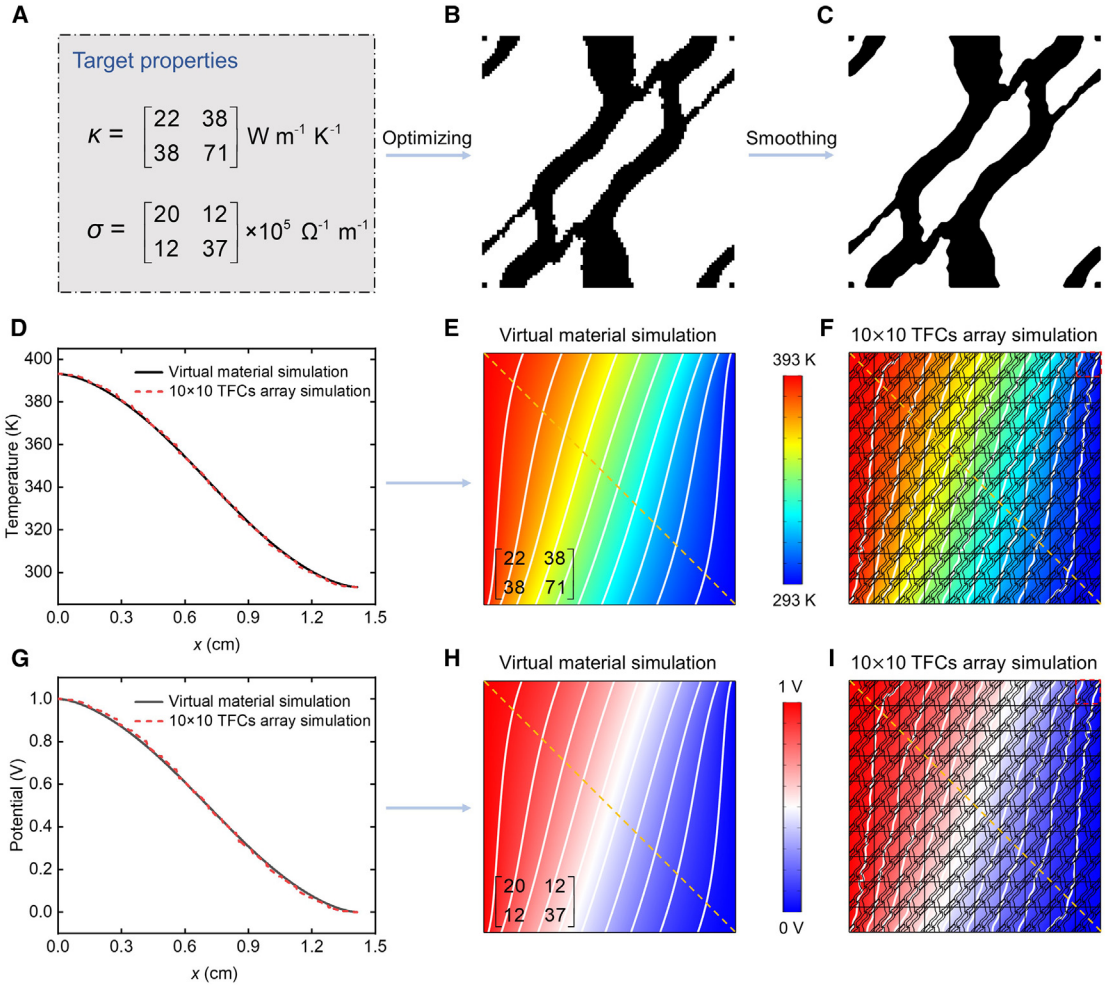

Figure 3. Numerical verification of the TFC

(A) Target properties κ and σ.

(B) Original TFC structure.

(C) Smoothed TFC structure.

(E and H) Thermal and electric fields of virtual materials with the target properties.

(F and I) Thermal and electric fields of 10 × 10 TFCs array.

(D and G) Temperature and potential comparisons along the orange dash line.

for storing the design variable. The thermal conductivity κ and electric conductivity σ of the background is set as 10 W m^{-1} K^{-1} and 2.5×10^6 Ω^{-1} m^{-1}. The properties of two materials in topology optimization are κ_1 = 1 W m^{-1} K^{-1}, σ_1 = 1.5 × 10^7 Ω^{-1} m^{-1} and κ_2 = 400 W m^{-1} K^{-1}, σ_2 = 10 Ω^{-1} m^{-1}. To design the arbitrary-shape cloak, we can map the outer parameterized curve $r \le R_2(\theta)$ into the inner one $R_1(\theta') \le r' \le R_2(\theta')$, as

$$\begin{cases} r' = \dfrac{R_2(\theta) - R_1(\theta)}{R_2(\theta)} r + R_1(\theta) \\ \theta' = \theta \end{cases} \quad \text{(Equation 5)}$$

The target conductivity ($\tilde{\kappa}$ and $\tilde{\sigma}$) $\tilde{\alpha}$ can be calculated as $\tilde{\alpha} = J\alpha_b J^T/\det(J)$, where J is the Jacobian matrix of the above coordinate transformation, α_b is the conductivity of the background and det(J) is the determinant of the matrix J. Combining the two formulas above, the target conductivity $\tilde{\alpha}$ in the intermediate region $R_1(\theta') \le r' \le R_2(\theta')$ can be deduced as

Cell Reports
Physical Science
Article

$$\begin{cases} \tilde{\alpha} = \begin{bmatrix} \tilde{\alpha}_{11} & \tilde{\alpha}_{12} \\ \tilde{\alpha}_{21} & \tilde{\alpha}_{22} \end{bmatrix} = \alpha_b \begin{bmatrix} \cos\varphi & -\sin\varphi \\ \sin\varphi & \cos\varphi \end{bmatrix} \begin{bmatrix} (\alpha_{11})_{r\theta} & (\alpha_{12})_{r\theta} \\ (\alpha_{21})_{r\theta} & (\alpha_{22})_{r\theta} \end{bmatrix} \begin{bmatrix} \cos\varphi & -\sin\varphi \\ \sin\varphi & \cos\varphi \end{bmatrix}^T \\ (\alpha_{11})_{r\theta} = \dfrac{(r' - R_1(\theta'))^2 + C^2}{r'(r' - R_1(\theta'))} \\ (\alpha_{12})_{r\theta} = (\alpha_{21})_{r\theta} = \dfrac{C}{r' - R_1(\theta')} \\ (\alpha_{22})_{r\theta} = \dfrac{r'}{r' - R_1(\theta')} \\ C = \dfrac{R_1(\theta')(r' - R_1(\theta'))\dfrac{dR_2(\theta')}{d\theta'} - R_2(\theta')(r' - R_2(\theta'))\dfrac{dR_1(\theta')}{d\theta'}}{R_2(\theta')(R_2(\theta') - R_1(\theta'))} \end{cases}$$

(Equation 6)

where φ is the azimuth coordinate.

To design the arbitrary-shape concentrator, the coordinate transformation formulas can be obtained by compressing the region $r \le R_3(\theta)$ into $r' \le R_1(\theta')$ and extending the region $R_3(\theta) \le r \le R_2(\theta)$ to $R_1(\theta') \le r' \le R_2(\theta')$. The mapping formulas are as follows:

$$\begin{cases} r' = r\dfrac{R_1(\theta)}{R_3(\theta)}, \theta' = \theta \; r' \le R_1(\theta') \\ r' = r\dfrac{R_2(\theta) - R_1(\theta)}{R_2(\theta) - R_3(\theta)} + \dfrac{R_2(\theta)(R_1(\theta) - R_3(\theta))}{R_2(\theta) - R_3(\theta)}, \theta' = \theta \; R_1(\theta') \le r' \le R_2(\theta') \end{cases}$$

(Equation 7)

The target conductivity $\tilde{\alpha}$ can be deduced in the same way. In the region $r' \le R_1(\theta')$,

$$\begin{cases} \tilde{\alpha} = \begin{bmatrix} \tilde{\alpha}_{11} & \tilde{\alpha}_{12} \\ \tilde{\alpha}_{21} & \tilde{\alpha}_{22} \end{bmatrix} = \alpha_b \begin{bmatrix} \cos\varphi & -\sin\varphi \\ \sin\varphi & \cos\varphi \end{bmatrix} \begin{bmatrix} (\alpha_{11})_{r\theta} & (\alpha_{12})_{r\theta} \\ (\alpha_{21})_{r\theta} & (\alpha_{22})_{r\theta} \end{bmatrix} \begin{bmatrix} \cos\varphi & -\sin\varphi \\ \sin\varphi & \cos\varphi \end{bmatrix}^T \\ (\alpha_{11})_{r\theta} = \dfrac{r'^2 + A^2}{r'^2}; \; (\alpha_{12})_{r\theta} = (\alpha_{21})_{r\theta} = \dfrac{A}{r'}; \; (\alpha_{22})_{r\theta} = 1 \\ A = \dfrac{r\left(R_2(\theta')\dfrac{dR_1(\theta')}{d\theta'} - R_1(\theta')\dfrac{dR_2(\theta')}{d\theta'}\right)}{R_2(\theta')R_1(\theta')} \end{cases}$$

(Equation 8)

In the region $R_1(\theta') \le r' \le R_2(\theta')$,

$$\begin{cases} \tilde{\alpha} = \begin{bmatrix} \tilde{\alpha}_{11} & \tilde{\alpha}_{12} \\ \tilde{\alpha}_{21} & \tilde{\alpha}_{22} \end{bmatrix} = \alpha_b \begin{bmatrix} \cos\varphi & -\sin\varphi \\ \sin\varphi & \cos\varphi \end{bmatrix} \begin{bmatrix} (\alpha_{11})_{r\theta} & (\alpha_{12})_{r\theta} \\ (\alpha_{21})_{r\theta} & (\alpha_{22})_{r\theta} \end{bmatrix} \begin{bmatrix} \cos\varphi & -\sin\varphi \\ \sin\varphi & \cos\varphi \end{bmatrix}^T \\ (\alpha_{11})_{r\theta} = \dfrac{(r' - b)^2 + A^2}{r'(r' - b)}; \; (\alpha_{12})_{r\theta} = (\alpha_{21})_{r\theta} = \dfrac{A}{r' - b}; \; (\alpha_{22})_{r\theta} = \dfrac{r'}{r' - b} \\ A = \dfrac{(R_2(\theta') - R_1(\theta'))(r' - R_2(\theta'))\dfrac{dR_3(\theta')}{d\theta'}}{(R_3(\theta') - R_1(\theta'))^2} + \\ \dfrac{(R_3(\theta') - R_1(\theta'))(r' - R_1(\theta'))\dfrac{dR_2(\theta')}{d\theta'} - (R_2(\theta') - R_3(\theta'))(r' - R_2(\theta'))\dfrac{dR_1(\theta')}{d\theta'}}{(R_3(\theta') - R_1(\theta'))^2} \\ b = \dfrac{R_2(\theta)(R_1(\theta) - R_3(\theta))}{R_2(\theta) - R_3(\theta)} \end{cases}$$

(Equation 9)

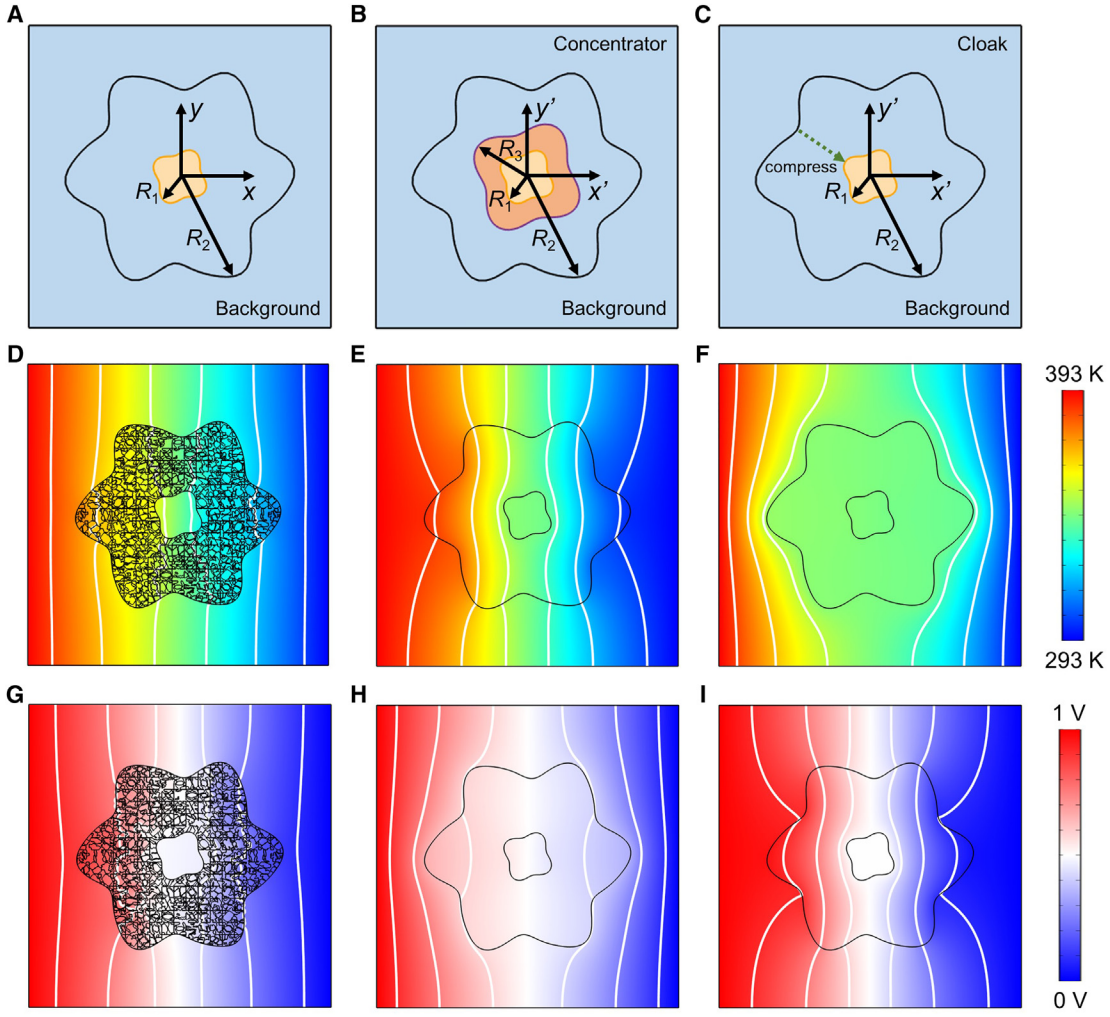

Figure 4. FCTO design of TMM with thermal concentrating and electric cloaking functions

(A) General geometry for the TMM.

(B) Coordinate transformation for a concentrator.

(C) Coordinate transformation for a cloak.

(D and G) Simulation of thermal concentrating and electric cloaking function.

(E and H) Simulation of temperature and electric fields when the design domain is filled with Material 1.

(F and I) Simulation of temperature and electric fields when the design domain is filled with Material 2.

Note that the target conductivity $\tilde{\alpha}$ is always an anisotropic tensor, resulting from the severe requirements of directional regulation, which is challenging to achieve with naturally occurring materials. A layer structure formed by alternating two materials is a decent option to achieve such anisotropic conductivity. However, this structure may not cover a sufficiently large conductivity space and achieve the target conductivity precisely due to its limited shapes and design freedoms. TFCs can achieve the target thermal and electric conductivities precisely since the materials distribution is obtained by iterative updating and is completely random, breaking the shape limitation and conductivity space of traditional layer structure.

As shown in Figures 4D and 4G, it is seen that good thermal concentrating and electric cloaking functions are obtained by referring to the enhanced thermal gradient and removed electric gradient inside the inner region encircled by the TMM, while

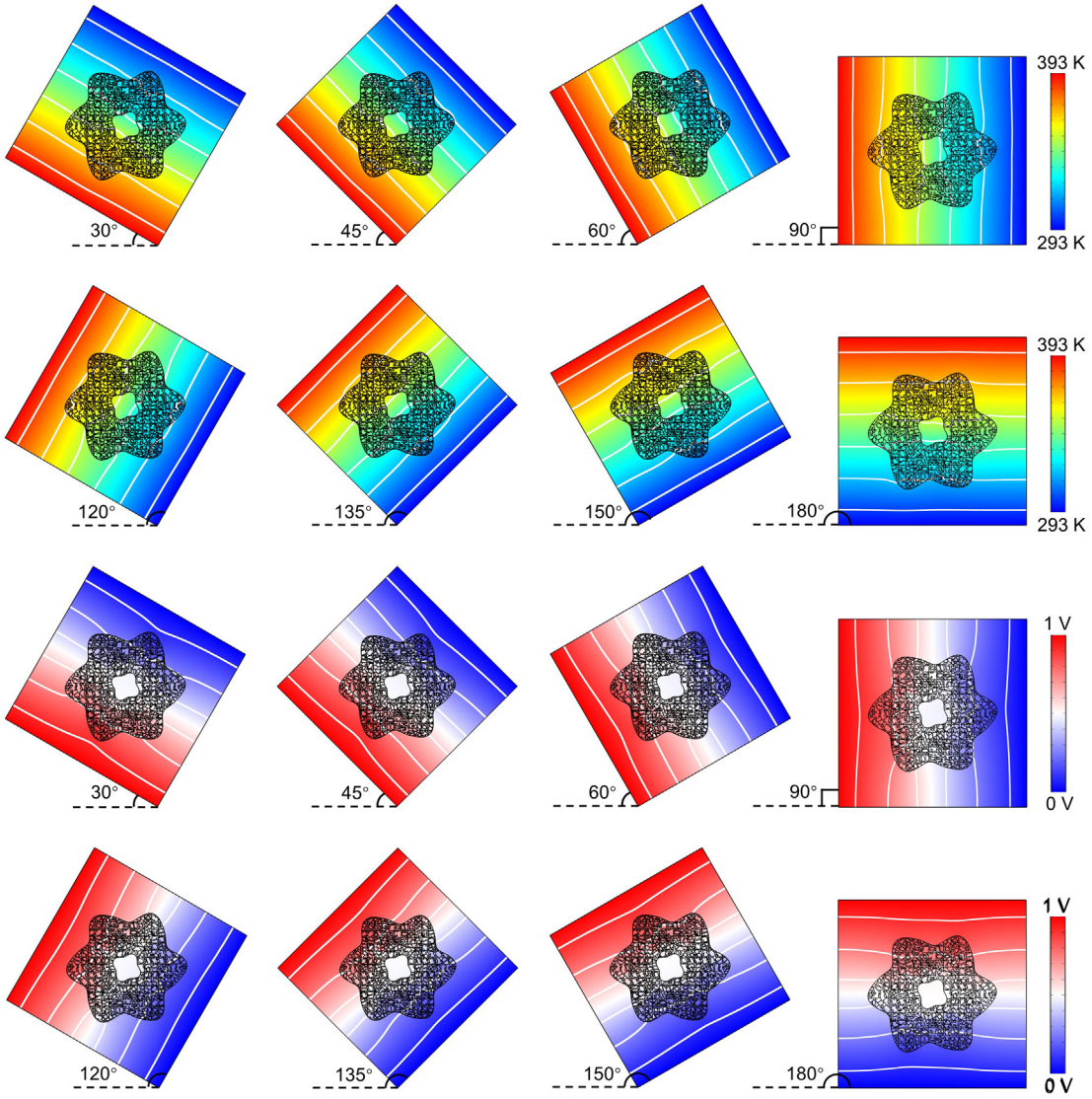

Figure 5. Simulation verifications of the designed multiphysics metamaterials under temperature/potential gradient with different directions

the thermal and electric fields outside the TMM keep almost unchanged. In contrast, when the TMM is filled with Materials 1 or 2, the thermal and electric fields are distorted obviously. Further, we demonstrated in Figure 5 that the designed TMM can maintain its thermal concentrating/electric cloaking functions omnidirectionally no matter in which direction the heat flux and electric current is projected. Besides the linear thermal/electric field gradient, the pre-designed functions maintain as well in the transient case and non-uniform source case in Figure S4.

Further, we would like to verify the performance with more different combinations of functions and shapes. As shown in Figure 6, we demonstrate the thermal cloaking/electric concentrating, thermal cloaking/electric cloaking, and thermal concentrating/electric concentrating functions as well. We design a same-shape TMM with above R_1, R_2, and R_3 shape for thermal cloaking/electric concentrating function in Figure 6A. It is seen that the thermal field gradient is removed while the electric

Please cite this article in press as: Zhu et al., Field-coupling topology design of general transformation multiphysics metamaterials with different functions and arbitrary shapes, Cell Reports Physical Science (2023), https://doi.org/10.1016/j.xcrp.2023.101540

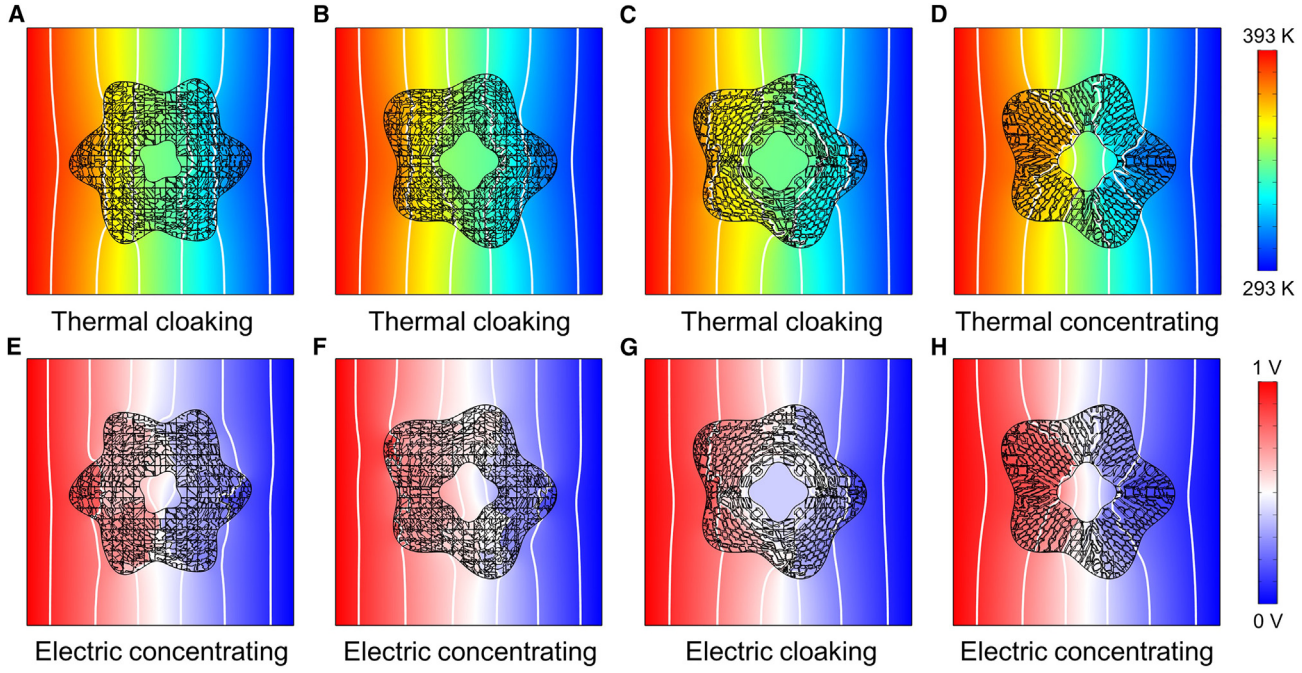

Figure 6. Demonstration of TMMs with different functions and different shapes

(A and E) TMM with thermal cloaking and electric concentrating function with the same shape as Figure 4.

(B and F) TMM with thermal cloaking and electric concentrating function with a different shape.

(C and G) TMM with thermal cloaking and electric cloaking functions.

(D and H) TMM with thermal concentrating and electric concentrating functions.

field gradient is enhanced inside the inner region, while the external fields are almost unchanged, verifying the good thermal cloaking/electric concentrating performance. In Figure 6B, we redesigned the TMM with different shapes by employing new parameterized curves as $R_1 = 0.75[2\,cos(4\theta) + 13]$ and $R_2 = 2[0.5\,sin(\theta) - sin(2\theta) - 0.5\,cos(\theta) + 2\,cos(5\theta) + 15]$. Similarly as in Figure 6A, very good thermal cloaking and electric concentrating functions are also observed. Further, we also designed two TMMs with the same functions as thermal/electric cloaking and concentrating functions in Figures 6C and 6D. In Figure 6C, both the thermal and electric field gradients are removed inside the inner region, verifying the good cloaking functions. In Figure 6D, both the thermal and electric field gradients are enhanced inside the inner region, demonstrating the good concentrating functions.

DISCUSSION

Finally, we would like to further discuss materials selection during the design of TMMs. For the same function in multiphysics fields, the requirement of material properties is constant $\tilde{\kappa}/\tilde{\sigma}$ according to Equation 1, which is relatively easy for selecting proper materials. Nevertheless, for different functions, according to Equation 2 the spatially varying $\tilde{\kappa}/\tilde{\sigma}$ makes it difficult to select proper materials for achieving the distinct $\tilde{\kappa}$ and $\tilde{\sigma}$ tensors. If we select the proper materials for achieving the same function, the error between the actual κ/σ and the target κ/σ is small and acceptable, as shown in Figure S5. But if we select the same materials for achieving different functions, the error is much larger and the optimized TFC has too many gray elements and disables the overall functions and practical fabrication. The distribution of constraints G between the effective properties and the target properties of the whole TMM with the same function and different functions is shown in Figure S6. It is seen that the error is much larger for different functions than the same function,

implying that the materials should be selected properly, especially for the different functions; otherwise the TFC cannot be fabricated and overall functions are far from satisfactory. In our study, we combine contradictory cloaking and concentrating functions into a single device because we try to solve the most challenging problem. To this end, we should select one material with low κ and high σ, and one material with high κ and low σ. Figure S7 shows the constraints G of two different TFCs with different material selections, implying the importance of material selections.

In summary, we propose a general roadmap to design arbitrary-shape TMM to manipulate heat and electric current simultaneously via FCTO for different functions. Based on FCTO, the desired thermal and electric anisotropic conductivity can be achieved effectively by designing TFCs, and subsequently the TMM can be obtained by assembling the TFCs according to the arbitrary shape. The robust manipulating of heat and electric current for different functions was validated no matter where the heat or electric current is input. The robust performance is inherited from the functionality-independent transformation theory. Compared with previous research on multiphysics metamaterials, our strategy advances in three aspects: (1) The present strategy can assist design multiphysics metamaterials with arbitrary shapes and different functions, which is the first time to deal with limited shapes and different functionality integration simultaneously. (2) With the high accuracy of FCTO, more materials, structures, shapes, and multiphysics functions can be designed under the general design framework. (3) Since all the TFCs are interconnected the multiphysics metamaterial is made into a whole, so the annoying thermal resistance issue is removed in our design. The discretion-and-assembly strategy of arbitrary-shape TMM is general, which can be used to design various TMMs beyond the demonstrated functions, like employing piezoelectric metamaterials to control the thermal-piezoelectric-mechanical properties.[44–46]The TMM is rather different from the previous bilayer or multiple concentric-ring structures, which offers great flexibility in terms of shape, functionality, and performance robustness, and removes the thermal resistance issue as we integrate all the TFCs into a single metadevice. Our study offers a general way to achieve metamaterials with anisotropic tensor properties and paves a new way to design TMM beyond the present thermotics and electrics.

EXPERIMENTAL PROCEDURES

Resource availability

Lead contact

Further information and requests should be directed to the lead contact, R. Hu (hurun@hust.edu.cn).

Materials availability

No experiments were performed in this study.

Data and code availability

All data generated by this study can be found in the article and supplemental information. Additional information is available from the corresponding author upon request.

SUPPLEMENTAL INFORMATION

Supplemental information can be found online at https://doi.org/10.1016/j.xcrp.2023.101540.

ACKNOWLEDGMENTS

R.H. would like to acknowledge the financial support of the National Natural Science Foundation of China (52076087, 5216110332, and 5221150005).

AUTHOR CONTRIBUTIONS

Z.Z., X.L., C.Q., and R.H. conceived the idea. Z.Z. and Z.W. performed the numerical simulations. Z.Z., T.L., and R.H. developed the code. Z.Z. and R.H. wrote the manuscript. All the authors contributed to the discussion and revision of the manuscript.

DECLARATION OF INTERESTS

The authors declare no competing interests.

Received: June 9, 2023
Revised: July 5, 2023
Accepted: July 19, 2023
Published: August 8, 2023

REFERENCES

1. Pendry, J.B., Schurig, D., and Smith, D.R. (2006). Controlling electromagnetic fields. Science *312*, 1780–1782. https://doi.org/10.1126/science.1125907.
2. Leonhardt, U. (2006). Optical conformal mapping. Science *312*, 1777–1780. https://doi.org/10.1126/science.1126493.
3. Chen, H., and Chan, C.T. (2007). Acoustic cloaking in three dimensions using acoustic metamaterials. Appl. Phys. Lett. *91*, 183518. https://doi.org/10.1063/1.2803315.
4. Li, J., Fok, L., Yin, X., Bartal, G., and Zhang, X. (2009). Experimental demonstration of an acoustic magnifying hyperlens. Nat. Mater. *8*, 931–934. https://doi.org/10.1038/NMAT2561.
5. Fan, C.Z., Gao, Y., and Huang, J.P. (2008). Shaped graded materials with an apparent negative thermal conductivity. Appl. Phys. Lett. *92*, 251907. https://doi.org/10.1063/1.2951600.
6. Guenneau, S., Amra, C., and Veynante, D. (2012). Transformation thermodynamics: cloaking and concentrating heat flux. Opt Express *20*, 8207–8218. https://doi.org/10.1364/OE.20.008207.
7. Chen, T., Weng, C.-N., and Chen, J.-S. (2008). Cloak for curvilinearly anisotropic media in conduction. Appl. Phys. Lett. *93*, 114103. https://doi.org/10.1063/1.2988181.
8. Narayana, S., and Sato, Y. (2012). Heat flux manipulation with engineered thermal materials. Phys. Rev. Lett. *108*, 214303. https://doi.org/10.1103/PhysRevLett.108.214303.
9. Schittny, R., Kadic, M., Guenneau, S., and Wegener, M. (2013). Experiments on transformation thermodynamics: molding the flow of heat. Phys. Rev. Lett. *110*, 195901. https://doi.org/10.1103/PhysRevLett.110.195901.
10. Li, Y., Li, W., Han, T., Zheng, X., Li, J., Li, B., Fan, S., and Qiu, C.-W. (2021). Transforming heat transfer with thermal metamaterials and devices. Nat. Rev. Mater. *6*, 488–507. https://doi.org/10.1038/s41578-021-00283-2.
11. Lei, M., Xu, L., and Huang, J. (2023). Spatiotemporal multiphysics metamaterials with continuously adjustable functions. Mater. Today Phys. *34*, 101057. https://doi.org/10.1016/j.mtphys.2023.101057.
12. Zhang, Z., Xu, L., Qu, T., Lei, M., Lin, Z.K., Ouyang, X., Jiang, J.H., and Huang, J. (2023). Diffusion metamaterials. Nat. Rev. Phys. *5*, 218–235. https://doi.org/10.1038/s42254-023-00565-4.
13. Jenett, B., Cameron, C., Tourlomousis, F., Rubio, A.P., Ochalek, M., and Gershenfeld, N. (2020). Discretely assembled mechanical metamaterials. Sci. Adv. *6*, eabc9943. https://doi.org/10.1038/s42254-023-00565-4.
14. Bauer, J., Meza, L.R., Schaedler, T.A., Schwaiger, R., Zheng, X., and Valdevit, L. (2017). Nanolattices: an emerging class of mechanical metamaterials. Adv. Mater. *29*, 1701850. https://doi.org/10.1002/adma.201701850.
15. Florijn, B., Coulais, C., and van Hecke, M. (2014). Programmable mechanical metamaterials. Phys. Rev. Lett. *113*, 175503. https://doi.org/10.1103/PhysRevLett.113.175503.
16. Han, T., Bai, X., Gao, D., Thong, J.T.L., Li, B., and Qiu, C.W. (2014). Experimental demonstration of a bilayer thermal cloak. Phys. Rev. Lett. *112*, 054302. https://doi.org/10.1103/PhysRevLett.112.054302.
17. Han, T., Yang, P., Li, Y., Lei, D., Li, B., Hippalgaonkar, K., and Qiu, C.W. (2018). Full-parameter omnidirectional thermal metadevices of anisotropic geometry. Adv. Mater. *30*, e1804019. https://doi.org/10.1002/adma.201804019.
18. Li, J., Li, Y., Li, T., Wang, W., Li, L., and Qiu, C.-W. (2019). Doublet thermal metadevice. Phys. Rev. Appl. *11*, 044021. https://doi.org/10.1103/PhysRevApplied.11.044021.
19. Su, Y., Li, Y., Yang, T., Han, T., Sun, Y., Xiong, J., Wu, L., and Qiu, C.W. (2021). Path-Dependent Thermal Metadevice beyond Janus Functionalities. Adv. Mater. *33*, 2003084. https://doi.org/10.1002/adma.202003084.
20. Xu, H., Shi, X., Gao, F., Sun, H., and Zhang, B. (2014). Ultrathin three-dimensional thermal cloak. Phys. Rev. Lett. *112*, 054301. https://doi.org/10.1103/PhysRevLett.112.054301.
21. Fujii, G., Akimoto, Y., and Takahashi, M. (2018). Exploring optimal topology of thermal cloaks by CMA-ES. Appl. Phys. Lett. *112*, 061108. https://doi.org/10.1063/1.5016090.
22. Zhu, Z., Ren, X., Sha, W., Xiao, M., Hu, R., and Luo, X. (2021). Inverse design of rotating metadevice for adaptive thermal cloaking. Int. J. Heat Mass Tran. *176*, 121417. https://doi.org/10.1016/j.ijheatmasstransfer.2021.121417.
23. Li, Y., Shen, X., Huang, J., and Ni, Y. (2016). Temperature-dependent transformation thermotics for unsteady states: Switchable concentrator for transient heat flow. Phys. Lett. *380*, 1641–1647. https://doi.org/10.1016/j.physleta.2016.02.040.
24. Shen, X., Li, Y., Jiang, C., Ni, Y., and Huang, J. (2016). Thermal cloak-concentrator. Appl. Phys. Lett. *109*, 031907. https://doi.org/10.1063/1.4959251.
25. Fujii, G., and Akimoto, Y. (2020). Cloaking a concentrator in thermal conduction via topology optimization. Int. J. Heat Mass Tran. *159*, 120082. https://doi.org/10.1016/j.ijheatmasstransfer.2020.120082.
26. Sha, W., Xiao, M., Zhang, J., Ren, X., Zhu, Z., Zhang, Y., Xu, G., Li, H., Liu, X., Chen, X., et al. (2021). Robustly printable freeform thermal metamaterials. Nat. Commun. *12*, 7228. https://doi.org/10.1038/s41467-021-27543-7.
27. Wang, Z., Zhu, Z., Liu, T., and Hu, R. (2022). Inverse design of thermal metamaterials with holey engineering strategy. J. Appl. Phys. *132*, 145102. https://doi.org/10.1063/5.0108743.
28. Guenneau, S., and Amra, C. (2013). Anisotropic conductivity rotates heat fluxes in transient regimes. Opt Express *21*, 6578–6583. https://doi.org/10.1364/OE.21.006578.

29. Hu, R., Zhou, S., Shu, W., Xie, B., Ma, Y., and Luo, X. (2016). Directional heat transport through thermal reflection meta-device. AIP Adv. *6*, 125111. https://doi.org/10.1063/1.4973309.

30. Hu, R., Zhou, S., Li, Y., Lei, D.Y., Luo, X., and Qiu, C.W. (2018). Illusion thermotics. Adv. Mater. *30*, 1707237. https://doi.org/10.1002/adma.201707237.

31. Sha, W., Zhao, Y., Gao, L., Xiao, M., and Hu, R. (2020). Illusion thermotics with topology optimization. J. Appl. Phys. *128*, 045106. https://doi.org/10.1063/5.0007354.

32. Xu, J., Zhang, J., Xiong, D., Lin, W., Wen, L., and Zhang, L. (2019). Creating illusion of discrete source array by simultaneously allocating thermal and DC fields with homogeneous media. Soft Matter *15*, 546–558. https://doi.org/10.1016/j.enconman.2019.03.056.

33. Li, Y., Bai, X., Yang, T., Luo, H., and Qiu, C.W. (2018). Structured thermal surface for radiative camouflage. Nat. Commun. *9*, 273. https://doi.org/10.1038/s41467-017-02678-8.

34. Liu, Y., Song, J., Zhao, W., Ren, X., Cheng, Q., Luo, X., Fang, N.X., and Hu, R. (2020). Dynamic thermal camouflage via a liquid-crystal-based radiative metasurface. Nanophotonics *9*, 855–863. https://doi.org/10.1515/nanoph-2019-0485.

35. Hu, R., Huang, S., Wang, M., Luo, X., Shiomi, J., and Qiu, C.W. (2019). Encrypted thermal printing with regionalization transformation. Adv. Mater. *31*, 1807849. https://doi.org/10.1002/adma.201807849.

36. Hu, R., Huang, S., Wang, M., Zhou, L., Peng, X., and Luo, X. (2018). Binary thermal encoding by energy shielding and harvesting units. Phys. Rev. Appl. *10*, 054032. https://doi.org/10.1103/PhysRevApplied.10.054032.

37. Ma, Y., Liu, Y., Raza, M., Wang, Y., and He, S. (2014). Experimental demonstration of a multiphysics cloak: manipulating heat flux and electric current simultaneously. Phys. Rev. Lett. *113*, 205501. https://doi.org/10.1103/PhysRevLett.113.205501.

38. Lan, C., Li, B., and Zhou, J. (2015). Simultaneously concentrated electric and thermal fields using fan-shaped structure. Opt Express *23*, 24475–24483. https://doi.org/10.1364/OE.23.024475.

39. Zhang, L., and Shi, Y. (2018). Bifunctional arbitrarily-shaped cloak for thermal and electric manipulations. Opt. Mater. Express *8*, 2600–2613. https://doi.org/10.1364/OME.8.002600.

40. Andreassen, E., and Andreasen, C.S. (2014). How to determine composite material properties using numerical homogenization. Comput. Mater. Sci. *83*, 488–495. https://doi.org/10.1016/j.commatsci.2013.09.006.

41. Sigmund, O. (2001). A 99 line topology optimization code written in Matlab. Struct. Multidiscip. Optim. *21*, 120–127. https://doi.org/10.1007/s001580050176.

42. Andreassen, E., Clausen, A., Schevenels, M., Lazarov, B.S., and Sigmund, O. (2011). Efficient topology optimization in MATLAB using 88 lines of code. Struct. Multidiscip. Optim. *43*, 1–16. https://doi.org/10.1007/s00158-010-0594-7.

43. Svanberg, K. (1987). The method of moving asymptotes—a new method for structural optimization. Int. J. Numer. Methods Eng. *24*, 359–373. https://doi.org/10.1002/nme.1620240207.

44. Cui, H., Yao, D., Hensleigh, R., Lu, H., Calderon, A., Xu, Z., Davaria, S., Wang, Z., Mercier, P., Tarazaga, P., and Zheng, X.R. (2022). Design and printing of proprioceptive three-dimensional architected robotic metamaterials. Science *376*, 1287–1293. https://doi.org/10.1126/science.abn0090.

45. Shi, X., von Weltin, E., Barr, J.L., and Unterwald, E.M. (2019). Architected cellular piezoelectric metamaterials: Thermo-electro-mechanical properties. Acta Mater. *151*, 91–102. https://doi.org/10.1016/j.actamat.2018.10.001.

46. Iyer, S., Alkhader, M., and Venkatesh, T. (2015). Electromechanical behavior of auxetic piezoelectric cellular solids. Scripta Mater. *99*, 65–68. https://doi.org/10.1016/j.scriptamat.2014.11.030.